Supplementary Information for

Fringe-mediated extension of *O*-linked fucose in the ligand-binding region of Notch1 increases binding to mammalian Notch ligands

Paul B. Taylor*[1], Hideyuki Takeuchi*[2], Devon Sheppard*[3], Chandramouli Chillakuri[1], Susan M. Lea[3], Robert S. Haltiwanger[2] and Penny A. Handford[#1]

1. Department of Biochemistry, University of Oxford, Oxford OX1 3QU
2. Department of Biochemistry and Cell Biology, Stony Brook University, Stony Brook, NY 11794-5215
3. Sir William Dunn School of Pathology, University of Oxford, Oxford OX1 3RE

*These authors contributed equally to this study

#For correspondence PAH penny.handford@bioch.ox.ac.uk Tel +44 1865 613260

BIOLOGICAL SCIENCES; Biochemistry

List of items

Supplementary Table 1. Functional consequences of Notch/ligand interactions

Supplementary Table 2. Crystallographic data

Figure S1. Mass spectra of glycopeptides modified with *O*-fucose glycans on T466 of hN1$_{11-13}$.

Figure S2. Stoichiometric modification of S458 at EGF12 and S496 at EGF13 of hN1$_{11-13}$ with *O*-glucose glycans.

Figure S3. Mass spectra of glycopeptides modified with *O*-glucose glycans on S458 in EGF12 of hN1$_{11-13}$.

Figure S4. Mass spectra of glycopeptides modified with *O*-glucose glycans on S496 in EGF13 of hN1$_{11-13}$.

Figure S5. Flow cytometry analysis of the effect of *O*-glucose modifications on binding to various Notch ligands.

Figure S6. Representative SPR trace for hJagged1NE3 injected over hN1$_{1-14}$Fc.

Figure S7. Raw SPR data for unmodified and O-fucose glycan modified hN1$_{11-13}$

Figure S8 SEC MALS analysis of unmodified and disaccharide modified hN1$_{11-13}$

Figure S9. Crystal packing for hN1$_{11-13}$ disaccharide

Figure S10. The effect of substituting T466 on binding to Jagged1.

Figure S11 NMR analysis of the calcium dependence of the major □-hairpin in hN1$_{11-13}$

Figure S12 Immunofluorescence images of the interaction between protein-coated fluorescent beads and Notch ligand-expressing cells.

Supplementary Table 1. Functional consequences of Notch/ligand interactions

	Ligand	Jagged1/Serrate		DLL1/Delta	
Receptor	Enzyme	Signalling	Binding	Signalling	Binding
Notch1	Lfng	-	+/=/-*	+	+
	Mfng	-	=	+	+
	Rfng	+/=†	=	+	+
dNotch	Fringe	-	-	+	+

Negative effect on binding/signalling (-). Positive effect (+). No change (=). d=*Drosophila*

* Large increase in binding of Jagged1-Fc to HEK293 cells expressing N1 [29], very mild/no increase in binding of Jagged1-Fc to 3T3 cells expressing N1 [27], or decrease in Jagged1-Fc binding to CHO cells expressing N1 [22]

† CSL-Luciferase reporter assay shows 2-fold increase in N1 activation by Jagged1 expressed on the surface of 3T3 cells, but no increase in activation by pre-clustered ligands [27].

Supplementary Table 2.

	mono-saccharide	di-saccharide	T466A	T466V	T466S
Space group	P31 2 1	P31 2 1	P 61 2 2	P 61 2 2	P 61 2 2
Cell					
a,b,c (Å)	28.4, 28.4, 282.9	28.4,28.4,282.4	62.6,62.6, 126.6	63.78, 63.78, 127.27	61.77, 61.77, 126.56
α, β, γ (Å)	90, 90, 120	90, 90, 120	90, 90, 120	90, 90, 120	90, 90, 120
Wavelength (Å)	0.917	0.917	1.746	0.98	0.98
Resolution (Å)	24.4-1.9(2.0-1.9)	47.1-1.6(1.7-1.6)	63.3-2.8(3.0-2.8)	50.7-3.0(3.1-3.0)	63.3-2.3(2.4-2.3)
R_{merge} (%)	6.8(41.8)	4.1(40.9)	11.8(44.4)	8.1(43.8)	6.7(55.0)
$I/\sigma I$	10.8(3.0)	15.3(2.3)	7.6(2.3)	10.2(2.8)	10.5(2.2)
Completeness (%)	93.5(95.3)	96.6(95.2)	99.0(99.9)	94.1(94.3)	97.2(98.4)
Redundancy	3.3	4.1	5.5	5	2.9
number reflections	10840	16974	3956	3174	6676
R_{work}/R_{free} (%)	22.4/26.0	23.2/27.0	22.5/26.5	26.0/28.2	25.6/28.6
Number of atoms					
protein	915	914	941	914	905
ligand/ion	14	28	26	4	13
water	55	141	13	1	5
B-factors	23.2	30.8	79.5	105.2	93
protein	23	28.7	80	105.4	93.2
ligand/ion	22.6	22.2	81	93.9	83.9
water	25.5	39.4	57.1	43.9	58.8
sugar	30	58.8			
rms deviation					
bond length (Å)	0.006	0.006	0.008	0.01	0.01
bond angles (°)	1.112	1.103	1.33	1.17	1.15
Residues in allowed regions of Ramachandran plot (%)	100	100	99.2	100	100
Residues in favoured regions of Ramachandran plot (%)	96.7	96.7	95.2	96.7	96.7

Figure S1

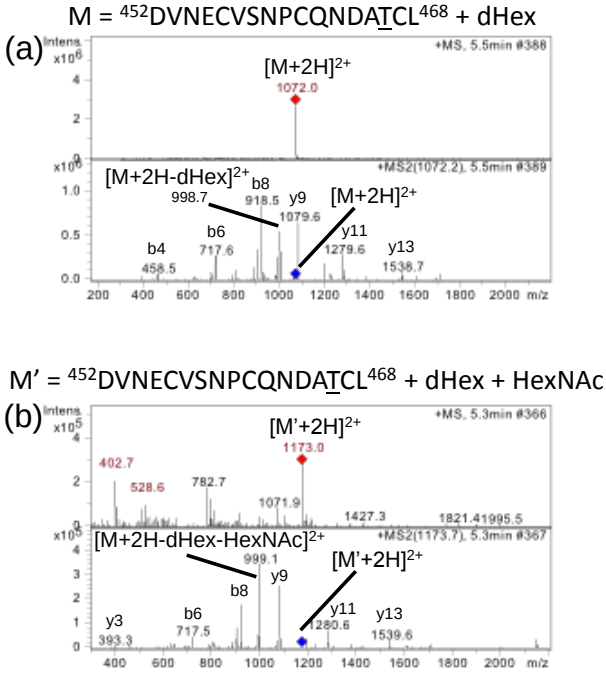

Figure S1. Mass spectra of glycopeptides modified with *O*-fucose glycans on T466 of $hN1_{11-13}$. **(a)** Asp-N-digested peptides generated from $hN1_{11-13}$ modified with an *O*-fucose monosaccharide (see Figure 1c) were analyzed by nano-liquid chromatography-electrospray ionization-MS/MS. Addition of an *O*-fucose monosaccharide was detected on the peptide ^{452}DVNECVSNPCQNDATCL^{468} from EGF12. The upper panel shows a full MS spectrum of material eluting at 5.5 min. The ion labelled $[M+2H]^{2+}$ matches the predicted mass for the doubly charged form of the *O*-fucosylated peptide (m/z 1071.8). Collision-induced dissociation fragmentation pattern of this ion is shown in the lower MS/MS panel. The parent ion selected for fragmentation in the MS spectrum is indicated by a red diamond. The position of the parent ion fragmented in the MS/MS spectrum is identified with a blue diamond. The ion, m/z 998.7 ($[M+2H\text{-dHex}]^{2+}$) matches the predicted mass (m/z 998.8) for the doubly charged, unglycosylated peptide. The difference between the mass of the parent ion (m/z 1071.8) and the product (m/z 998.7) matches the loss of a deoxyhexose (dHex, presumably a fucose, 146 Da) during the fragmentation of a doubly charged peptide (73 Da x 2 =146 Da). Confirmation of the peptide as ^{452}DVNECVSNPCQNDATCL^{468} comes from detection of a number of b and y ions indicated in the MS/MS spectrum. EIC in Figure 1g were done with m/z 1071.8 for *O*-fucose mono- and m/z 1173.3 for di-saccharide glycoforms, and m/z 998.8 for the unmodified form of the peptide. **(b)** Asp-N-digested peptides generated from $hN1_{11-13}$ modified with an *O*-fucose disaccharide (see Figure 1d) by nano-liquid chromatography-electrospray ionization-MS/MS. Addition of an *O*-fucose disaccharide was detected on the peptide ^{452}DVNECVSNPCQNDATCL^{468} from EGF12. The upper panel shows a full MS spectrum of material eluting at 5.3 min. The ion labelled $[M'+2H]^{2+}$ matches the predicted mass for the doubly charged form of the peptide with an *O*-fucose disaccharide (m/z 1173.3). Collision-induced dissociation fragmentation pattern of this ion is shown in the lower MS/MS panel. The parent ion selected for fragmentation in the MS spectrum is indicated by a red diamond. The position of the parent ion fragmented in the MS/MS spectrum is identified with a blue diamond. The ion, m/z 999.1 ($[M'+2H\text{-dHex-HexNAc}]^{2+}$) matches the predicted mass (m/z 998.8) for the doubly charged, unglycosylated peptide. The difference between the mass of the parent ion (m/z 1173.7) and the product (m/z 999.1) matches the loss of both a deoxyhexose (dHex, presumably a fucose, 146 Da) and an *N*-acetylhexsosamine (HexNAc, presumably a GlcNAc, 203 Da) during the fragmentation of a doubly charged peptide (174.6 Da x 2 =349.2 Da). Confirmation of the peptide as ^{452}DVNECVSNPCQNDATCL^{468} comes from detection of a number of b and y ions indicated in the MS/MS spectrum. EIC in Figure 1h were done with m/z 1173.3 for *O*-fucose disaccharide glycoform, m/z 1071.8 for *O*-fucose monosaccharide glycoform, and m/z 998.8 for the unmodified form.

Figure S2

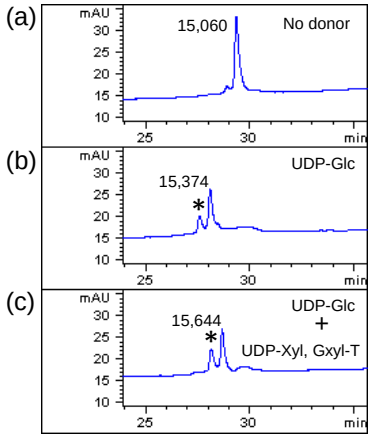

Figure S2. Stoichiometric modification of S458 at EGF12 and S496 at EGF13 of hN1$_{11\text{-}13}$ with *O*-glucose glycans. Synthesis of *O*-glucose mono- (b) and disaccharide (c) forms of hN1$_{11\text{-}13}$. Since Poglut utilizes UDP-xylose (Xyl) as well we UDP-glucose (Glc), UDP-Xyl and Glucoside xylosyltransferase (Gxyl-T) were added after completion of *O*-glucosylation at EGF12 and EGF13 by Poglut. Representative HPLC profiles of hN1$_{11\text{-}13}$ incubated with Poglut in the absence of donor **(a)** or the presence of UDP-Glc **(b)** are shown. **(c)** After overnight incubation, UDP-Xyl and recombinant Gxyl-T were added and further incubated. The masses of the species in each peak as determined by mass spectrometry are shown. mAU indicates milli-absorbance units. * indicates oxidized species.

Figure S3 *O*-Glucosylation at EGF12

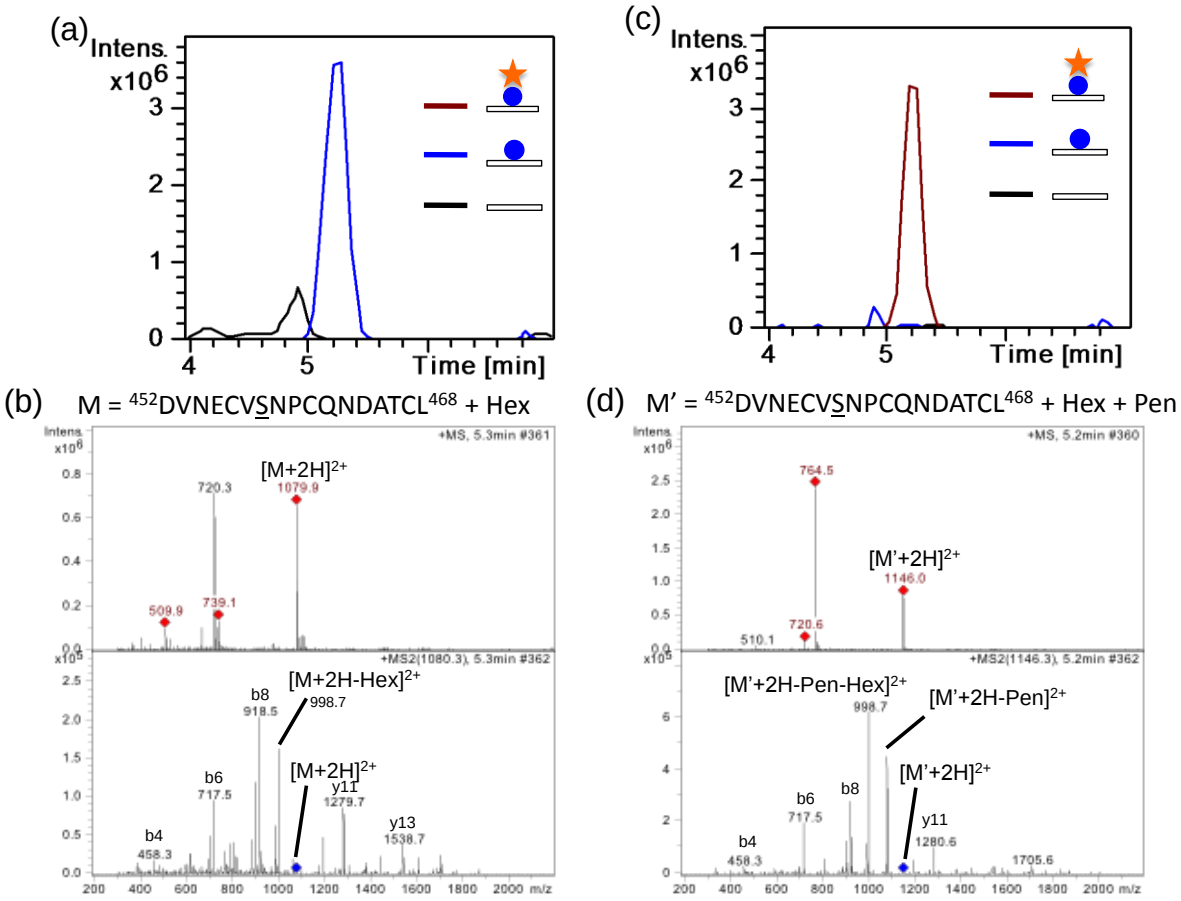

Figure S3. Mass spectra of glycopeptides modified with *O*-glucose glycans on S458 in EGF12 of hN1$_{11\text{-}13}$. (a) EICs of the ions corresponding to glycoforms of the peptide, ^{452}DVNECVSNPCQNDATCL^{468}, containing the *O*-glucose consensus sequence from EGF12 derived from Asp-N digests of hN1$_{11\text{-}13}$ modified with *O*-glucose monosaccharide (from Figure S2b). The MS data were searched for the doubly charged form of the (glyco)peptides: m/z 998.8 for the unglycosylated (black), m/z 1079.8 for the *O*-glucose monosaccharide (blue), and m/z 1145.8 for the *O*-glucose disaccharide glycoform (brown). **(b)** Asp-N-digested peptides generated from hN1$_{11\text{-}13}$ modified with *O*-glucose monosaccharides by nano-liquid chromatography-electrospray ionization-MS/MS. Addition of an *O*-glucose monosaccharide was detected on the peptide ^{452}DVNECVSNPCQNDATCL^{468} from EGF12. The upper panel shows a full MS spectrum of material eluting at 5.3 min. The ion labelled $[M+2H]^{2+}$ matches the predicted mass for the doubly charged form of the *O*-glucosylated peptide (m/z 1079.8). Collision-induced dissociation fragmentation pattern of this ion is shown in the lower MS/MS panel. The parent ion selected for fragmentation in the MS spectrum is indicated by a red diamond. The position of the parent ion fragmented in the MS/MS spectrum is identified with a blue diamond. The major ion, m/z 998.7 ($[M+2H\text{-}Hex]^{2+}$) matches the mass for the unglycosylated peptide. The difference between the mass of the parent ion (m/z 1080.3) and the product (m/z 998.7) matches the loss of a hexose (Hex, presumably a glucose, 162 Da) during the fragmentation of a doubly charged peptide (81.6 Da x 2 =163.2 Da). Confirmation of the peptide as ^{452}DVNECVSNPCQNDATCL^{468} comes from detection of a number of b and y ions indicated in the MS/MS spectrum. **(c)** EICs of the ions corresponding to glycoform of the peptide, ^{452}DVNECVSNPCQNDATCL^{468}, containing the *O*-glucose consensus sequence from EGF12 derived from Asp-N digests of hN1$_{11\text{-}13}$ modified with *O*-glucose disaccharide (from Figure S2c). The MS data were searched for the doubly charged form of the (glyco)peptides: m/z 998.8 for the unglycosylated form (black), m/z 1145.8 for the *O*-glucose disaccharide form (brown), and m/z 1079.8 for the *O*-glucose monosaccharide form (blue). **(d)** Asp-N-digested peptides generated from hN1$_{11\text{-}13}$ modified with *O*-glucose disaccharides by nano-liquid chromatography-electrospray ionization-MS/MS. Addition of an *O*-glucose disaccharide was detected on the peptide ^{452}DVNECVSNPCQNDATCL^{468} from EGF12. The upper panel shows a full MS spectrum

of material eluting at 5.2 min. The ion labelled $[M'+2H]^{2+}$ matches the predicted mass for the doubly charged form of the *O*-glucosylated peptide (m/z 1145.8). Collision-induced dissociation fragmentation pattern of this ion is shown in the lower MS/MS panel. The parent ion selected for fragmentation in the MS spectrum is indicated by a red diamond. The position of the parent ion fragmented in the MS/MS spectrum is identified with a blue diamond. The major ion, m/z 998.7 ($[M'+2H\text{-Pen-Hex}]^{2+}$) matches the mass for the unglycosylated peptide. The difference between the mass of the parent ion (m/z 1146.3) and the product (m/z 998.7) matches the loss of a pentose (Pen) and a hexose (Hex) which are presumably a xylose (132 Da) and a glucose (162 Da) during the fragmentation of a doubly charged peptide (147.6 Da x 2 =295.2 Da). Confirmation of the peptide as ^{452}DVNECVSNPCQNDATCL^{468} comes from detection of a number of b and y ions indicated in the MS/MS spectrum.

Figure S4 *O*-Glucosylation at EGF13

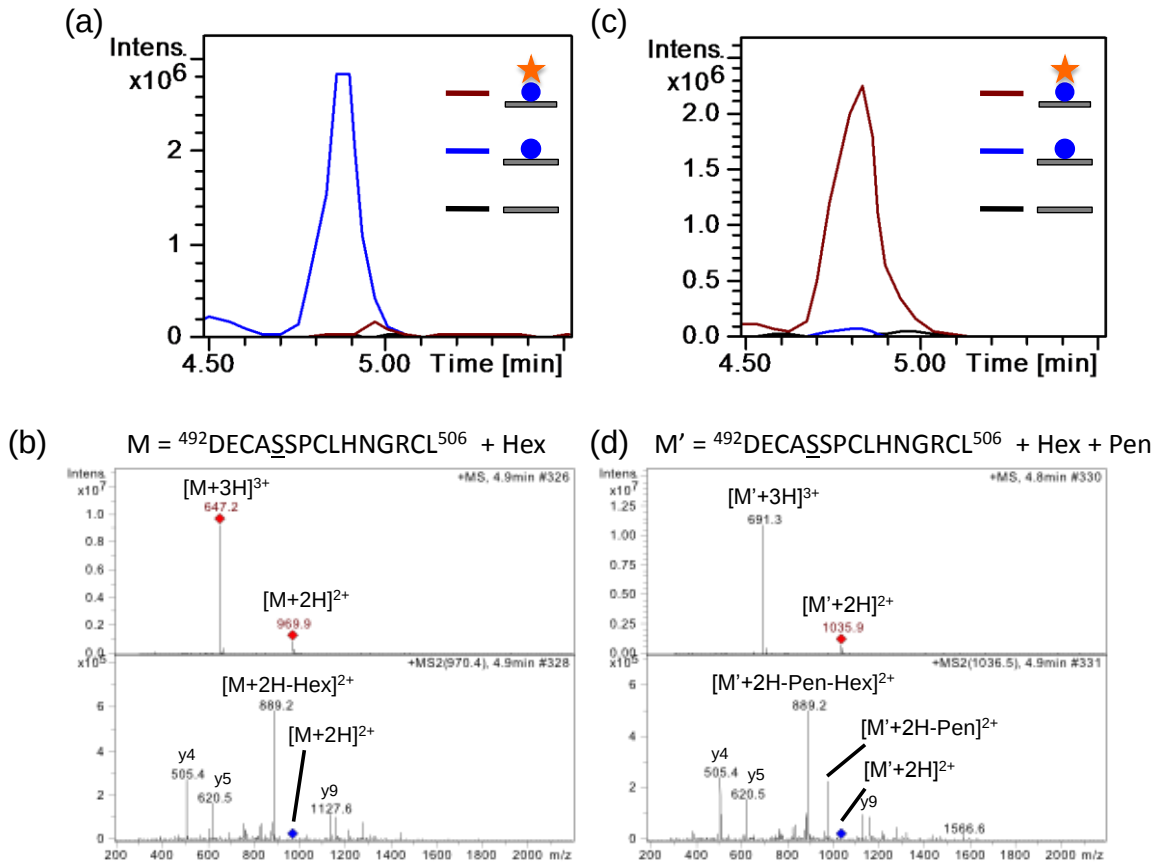

Figure S4. Mass spectra of glycopeptides modified with *O*-glucose glycans on S496 in EGF13 of hN1$_{11\text{-}13}$. (a) EICs of the ions corresponding to glycoforms of the peptide, ^{492}DECASSPCLHNGRCL^{506}, containing the *O*-glucose consensus sequence from EGF13 derived from Asp-N digests of hN1$_{11\text{-}13}$ modified with *O*-glucose monosaccharide (from Figures S2b). The MS data were searched for the doubly charged form of the (glyco)peptides: m/z 888.7 for the unglycosylated form (black), m/z 969.7 for the *O*-glucose monosaccharide glycoform (blue), and m/z 1035.7 for the *O*-glucose disaccharide glycoform (brown). **(b)** Asp-N-digested peptides generated from hN1$_{11\text{-}13}$ modified with *O*-glucose monosaccharides by nano-liquid chromatography-electrospray ionization-MS/MS. Addition of an *O*-glucose monosaccharide was detected on the peptide ^{492}DECASSPCLHNGRCL^{506} from EGF13. The upper panel shows a full MS spectrum of material eluting at 4.9 min. The ions labelled $[M+2H]^{2+}$ (m/z 969.9) and $[M+3H]^{3+}$ (m/z 647.2) match the predicted masses for the doubly and triply charged forms of the *O*-glucosylated peptide, respectively. Collision-induced dissociation fragmentation pattern of the doubly charged ion is shown in the lower MS/MS panel. The parent ion selected for fragmentation in the MS spectrum is indicated by a red diamond. The position of the parent ion fragmented in the MS/MS spectrum is identified with a blue diamond. The major ion, m/z 889.2 ($[M+2H\text{-}Hex]^{2+}$) matches the mass for the unglycosylated peptide. The difference between the mass of the parent ion (m/z 970.4) and the product (m/z 889.2) matches the loss of a hexose (Hex) which is presumably a glucose (162 Da) during the fragmentation of a doubly charged peptide (81.2 Da x 2 =162.4 Da). Confirmation of the peptide as ^{92}DECASSPCLHNGRCL^{506} comes from detection of a number of b and y ions indicated in the MS/MS spectrum. **(c)** EICs of the ions corresponding to glycoforms of the peptide, ^{492}DECASSPCLHNGRCL^{506}, containing the *O*-glucose consensus sequence from EGF13 derived from Asp-N digests of hN1$_{11\text{-}13}$ modified with *O*-glucose disaccharide (see Figure S2c). The MS data were searched for the doubly charged form of the (glyco)peptides: m/z 888.7 for the unglycosylated form (black), m/z 969.7 for the *O*-glucose monosaccharide form (blue), and m/z 1035.7 for the *O*-glucose disaccharide form (brown). **(d)** Asp-N-digested peptides generated from hN1$_{11\text{-}13}$ modified with *O*-glucose disaccharides by nano-liquid chromatography-electrospray

ionization-MS/MS. Addition of an *O*-glucose disaccharide was detected on the peptide ^{492}DECASSPCLHNGRCL^{506} from EGF13. The upper panel shows a full MS spectrum of material eluting at 4.8 min. The ion labelled $[M'+2H]^{2+}$ (m/z 1035.9) and $[M'+3H]^{3+}$ (m/z 691.3) match the predicted mass for the doubly and triply charged forms of the *O*-glucosylated peptide, respectively. Collision-induced dissociation fragmentation pattern of the doubly charged ion is shown in the lower MS/MS panel. The parent ion selected for fragmentation in the MS spectrum is indicated by a red diamond. The position of the parent ion fragmented in the MS/MS spectrum is identified with a blue diamond. The major ion, m/z 889.2 ($[M'+2H-Pen-Hex]^{2+}$) matches the mass for the unglycosylated peptide. The difference between the mass of the parent ion (m/z 1036.5) and the product (m/z 889.2) matches the loss of a pentose (Pen) which is presumably a xylose (132 Da) and a hexose (Hex) which is presumably a glucose (162 Da) during the fragmentation of a doubly charged peptide (147.3 Da x 2 =294.6 Da). Confirmation of the peptide as ^{492}DECASSPCLHNGRCL^{506} comes from detection of a number of b and y ions indicated in the MS/MS spectrum.

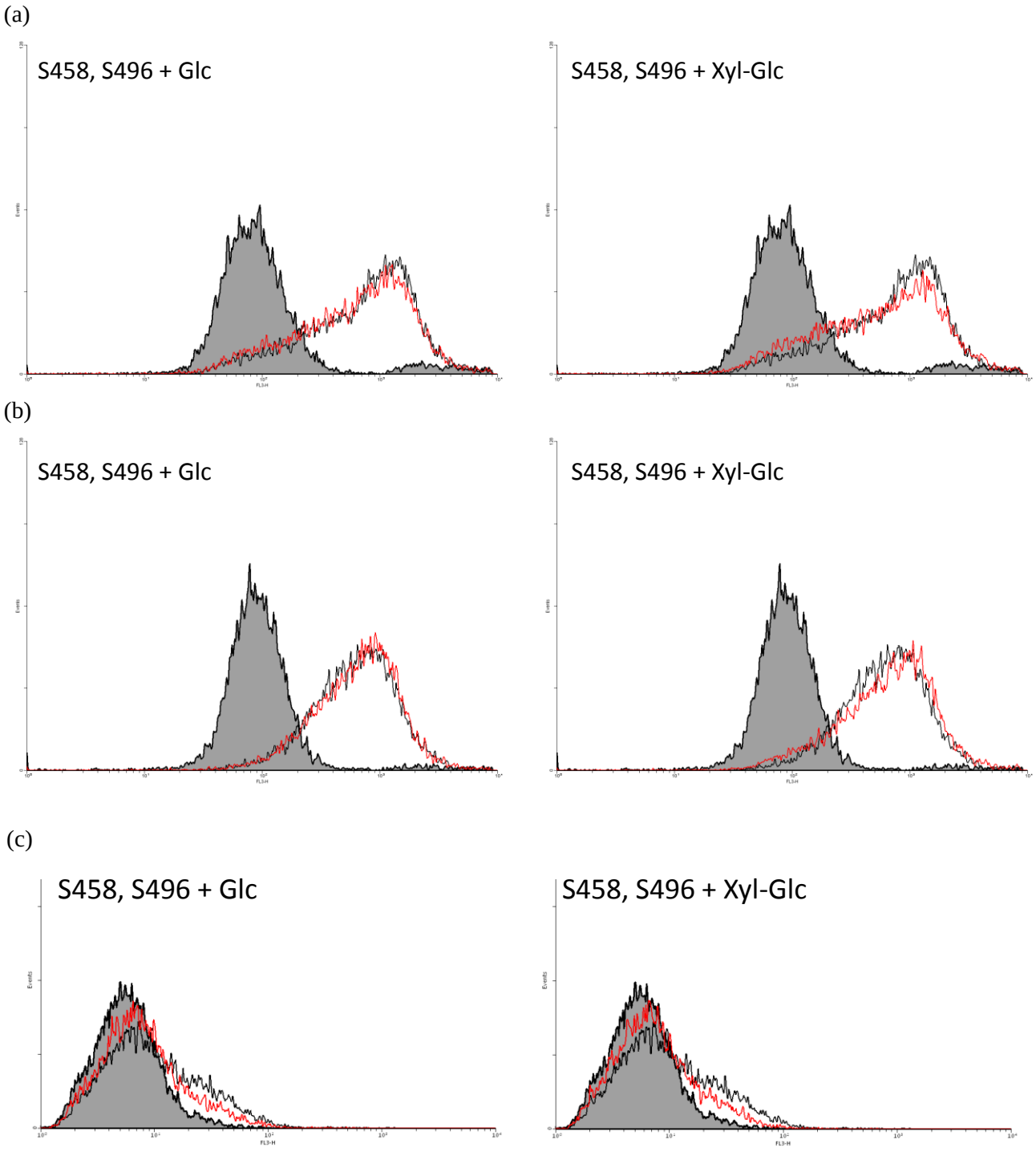

Figure S5. Flow cytometry analysis of the effect of *O*-glucose modifications on binding to various Notch ligands. Flow cytometry of **(a)** B16 cells expressing Jagged1, **(b)** B16 cells expressing DLL4, or **(c)** CHO cells expressing DLL1 after interaction with biotinylated $hN1_{11-13}$ modified with various sugars at S458 and S496 (red line) bound to avidin-coated fluorescent beads. In each case a negative control (fibrillin-1 $cbEGF_{12-14}$, grey shading) and positive control ($hN1_{11-13}$ WT, black line) are shown. In each case a representative trace is shown. Neither the addition of the *O*-glucose monosaccharide, nor the xylose-glucose had any effect on binding to any of the ligands.

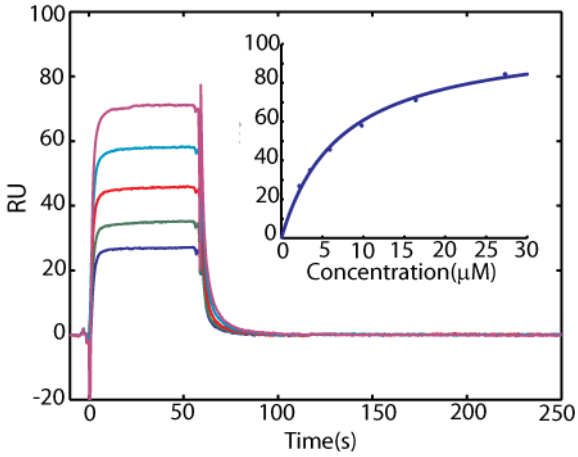

Figure S6. Representative SPR trace for hJagged1NE3 injected over $hN1_{1-14}$Fc. An SPR binding assay was developed to study the interaction between Notch and its ligands. $hN1_{1-14}$-Fc was immobilised on the chip, and a titration was performed using monomeric $hJagged1_{NE3}$ as an analyte. Equilibrium binding was measured over a range of concentrations, and a K_d of 7.1 +/- 0.1 μM was calculated using a 1:1 binding model. $hJagged1_{NE3}$ was injected at concentrations from 2.2-27.3 μM at 10μl/min in duplicate over immobilised $hN1_{1-14}$. The K_D was fit using a 1:1 steady-state model and averaged over multiple channels and titrations.

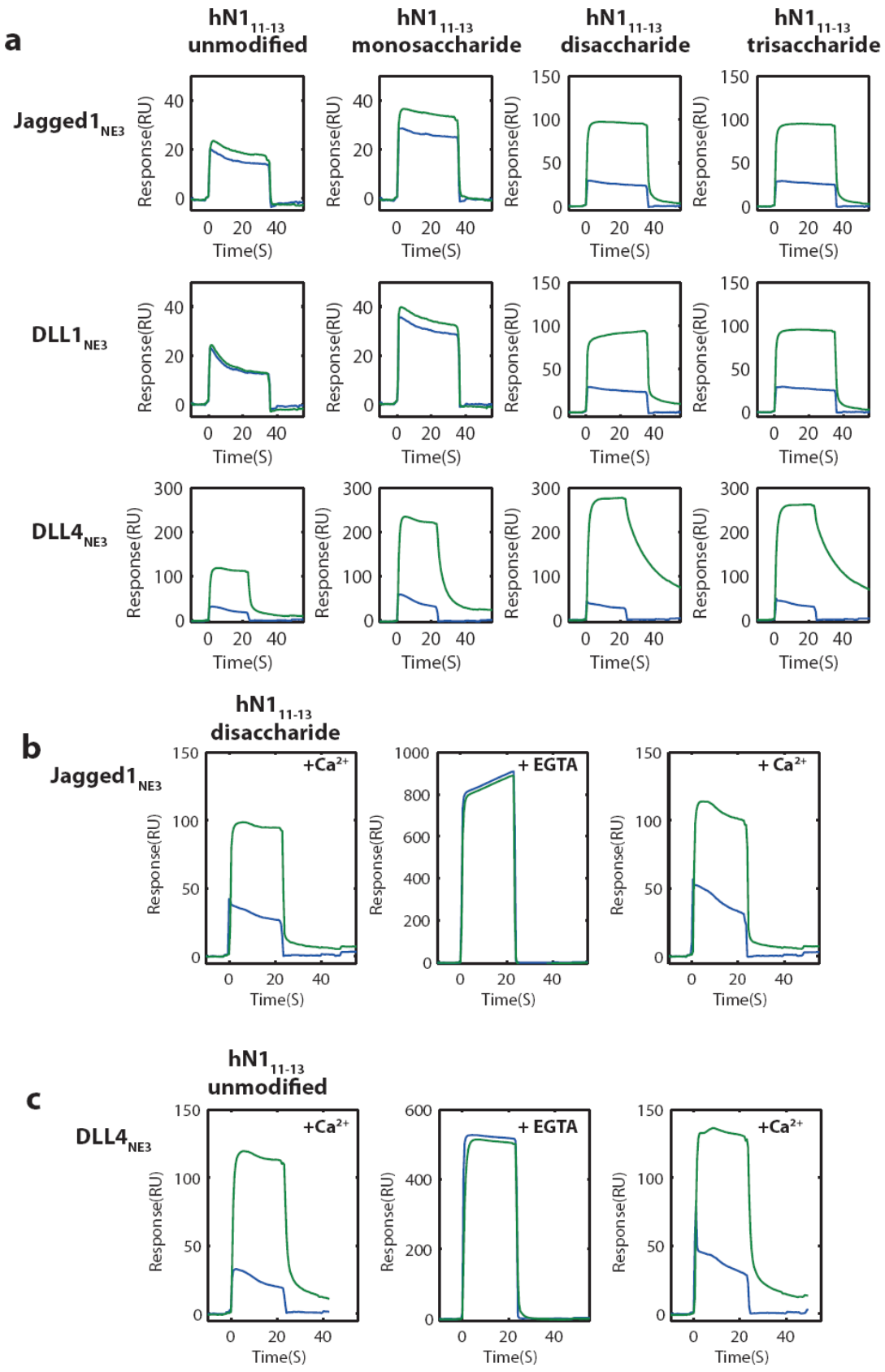

Figure S7. SPR traces for Notch-ligand binding (a) Raw SPR traces for Jagged1$_{NE3}$-Fc, DLL1$_{NE3}$-Fc, DLL4$_{NE3}$-Fc (+Notch channel in green, control channel (no ligand) in blue) with 10μM hN1$_{11-13}$ variants injected. **(b)** Calcium dependence of hN1$_{11-13}$ disaccharide binding to Jagged1$_{NE3}$-Fc. Injections of hN1$_{11-13}$ were done sequentially with the addition of 1mM $CaCl_2$, 10mM EGTA and repeated with 1mM $CaCl_2$. **(c)** Calcium dependence of hN1$_{11-13}$ unmodified binding to DLL4$_{NE3}$-Fc. Injections of hN1$_{11-13}$ were done sequentially with the addition of 1mM $CaCl_2$, 10mM EGTA and repeated with 1mM $CaCl_2$.

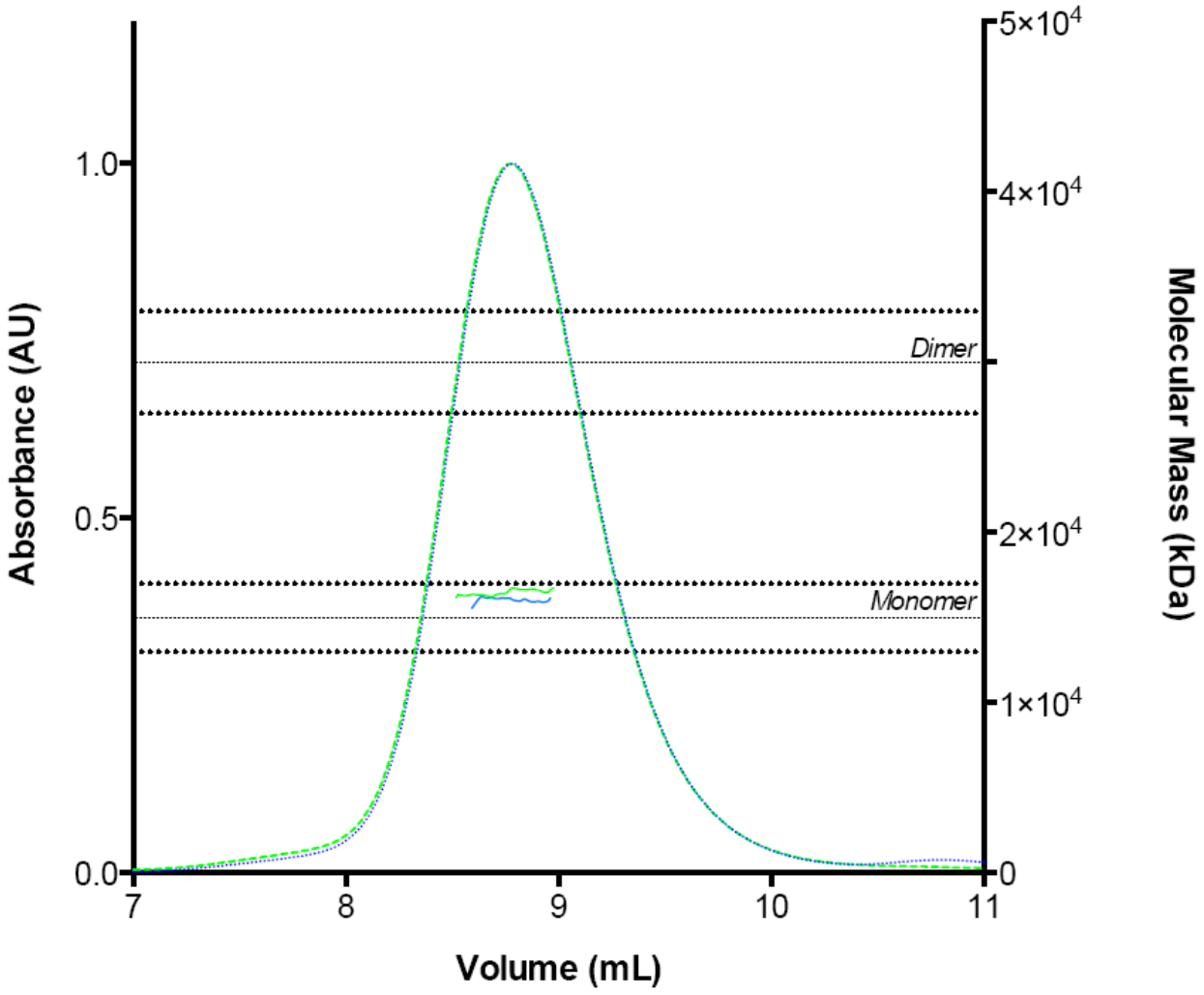

Figure S8. SEC-MALS analysis of unmodified (blue) and disaccharide-modified (green) hN1 $_{11\text{-}13}$ demonstrates that both forms of the protein are monomeric at the concentrations tested. Size exclusion chromatography was performed on a Superdex 200 5/150 column (GE Healthcare) equilibrated in HBS-CP (10mM HEPES pH7.4, 150mM NaCl, 1mM $CaCl_2$, 0.005% (v/v) Surfactant P20). 25ul of protein was injected at approx 1mg/ml and eluted at 0.25ml/min. The column was followed in line by a Dawn Heleos-II light scattering detector (Wyatt Technologies) and an Optilab-Rex refractive index monitor (Wyatt Technologies). Molecular mass calculations were performed using ASTRA 6.1.1.17 (Wyatt Technologies) assuming a dn/dc value of 0.186 ml/g.

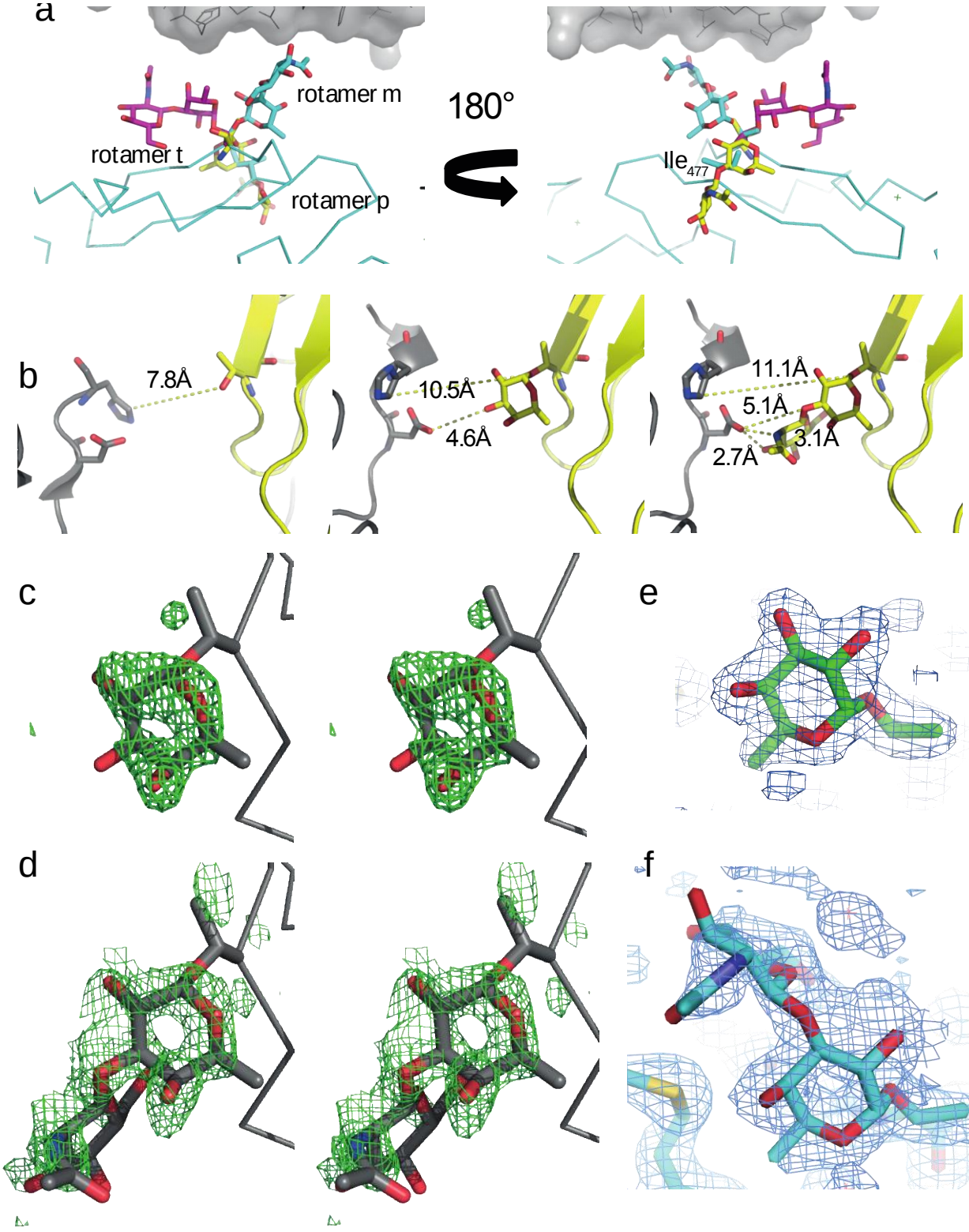

Figure S9. Crystal packing for hN1$_{11\text{-}13}$ disaccharide **(a)** Human N1$_{11\text{-}13}$ disaccharide shown with the three most commonly observed side chain rotamer conformations, p (49%), m(43%), t(7%) for Thr$_{466}$. The closest neighbouring molecule in the crystal lattice to this site is shown as a grey surface representation. Ile$_{477}$ clashes with the most commonly observed side chain rotamer p. While both m and t rotamers are potentially accessible only the m conformation is observed. **(b)** Closest contacts are shown for the unglycosylated, monosaccharide and disaccharide X-ray structures respectively, the most closely packed molecule within the crystal is shown in grey. Stereo electron density simulated annealing omit maps contoured at 3σ for **(c)** monosaccharide and **(d)** disaccharide hN1$_{11\text{-}13}$ and mono 2Fo-Fc maps for the final model contoured at 1σ are shown in panels **(e)** monosaccharide and **(f)** disaccharide.

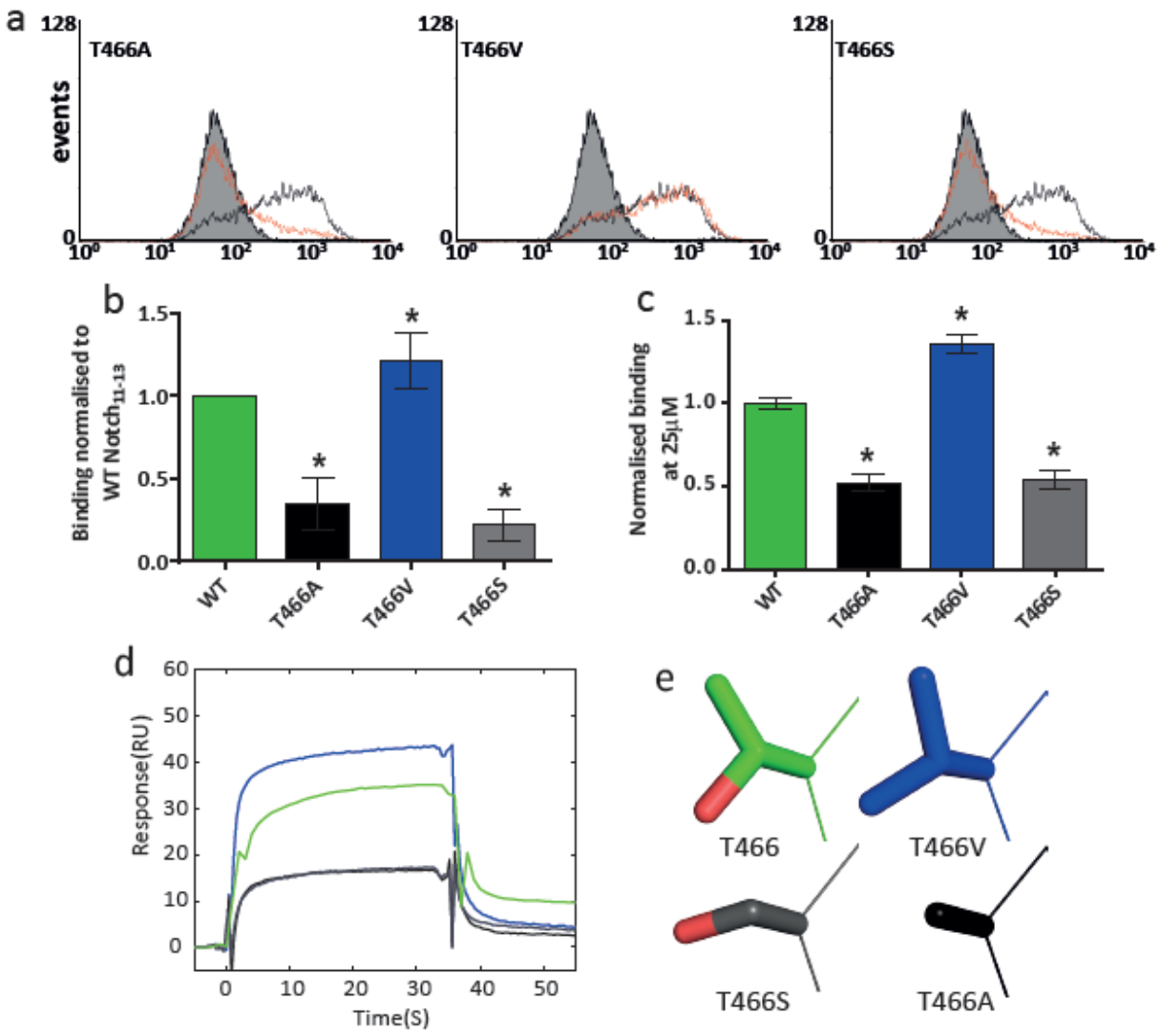

Figure S10. The effect of substituting T466 on binding to Jagged1. **(a)** Flow cytometry of B16 cells expressing Jagged1 after interaction with biotinylated $hN1_{11\text{-}13}$ mutants (red line) bound to avidin-coated fluorescent beads. In each case a representative trace is shown. Binding of the three mutant constructs (red line) is compared with a negative control (fibrillin-1 $cbEGF_{12\text{-}14}$, grey shading) and positive control ($hN1_{11\text{-}13}$ WT, black line). The T466A and T466S substitutions caused a substantial reduction in binding, compared to WT (indicated by the leftwards shift of the fluorescence profile compared with the positive control). By contrast the T466V substitution caused a slight increase in binding. **(b)** FACS binding data normalized to WT $N1_{11\text{-}13}$. Increased or attenuated binding for T466A, T466V and T466S was found to be significant (*) by Tukey's multiple comparison test ($p<0.0001$, $p=0.0369$, $p<0.0001$). **(c)** SPR binding of $Notch1_{11\text{-}13}$ T466 mutants to $hJagged1_{NE3}$-Fc normalized to $hN1_{11\text{-}13}$ WT at 25 μM with standard deviation shown. All differences to WT were found to be significant (*) by Tukey's multiple comparison test ($p<0.0001$). **(d)** Representative SPR traces for binding of 25 μM of the unmodified (green), T466A (black), T466V (blue) and T466S (grey) $hN1_{11\text{-}13}$ constructs over ~4500 RU $Jagged1_{NE3}$-Fc. Traces were corrected for refractive index changes by subtraction of a control trace (see Materials and methods) **(e)** Conformation of T466, T466V, T466S, T466A from superimposed X-ray structures.

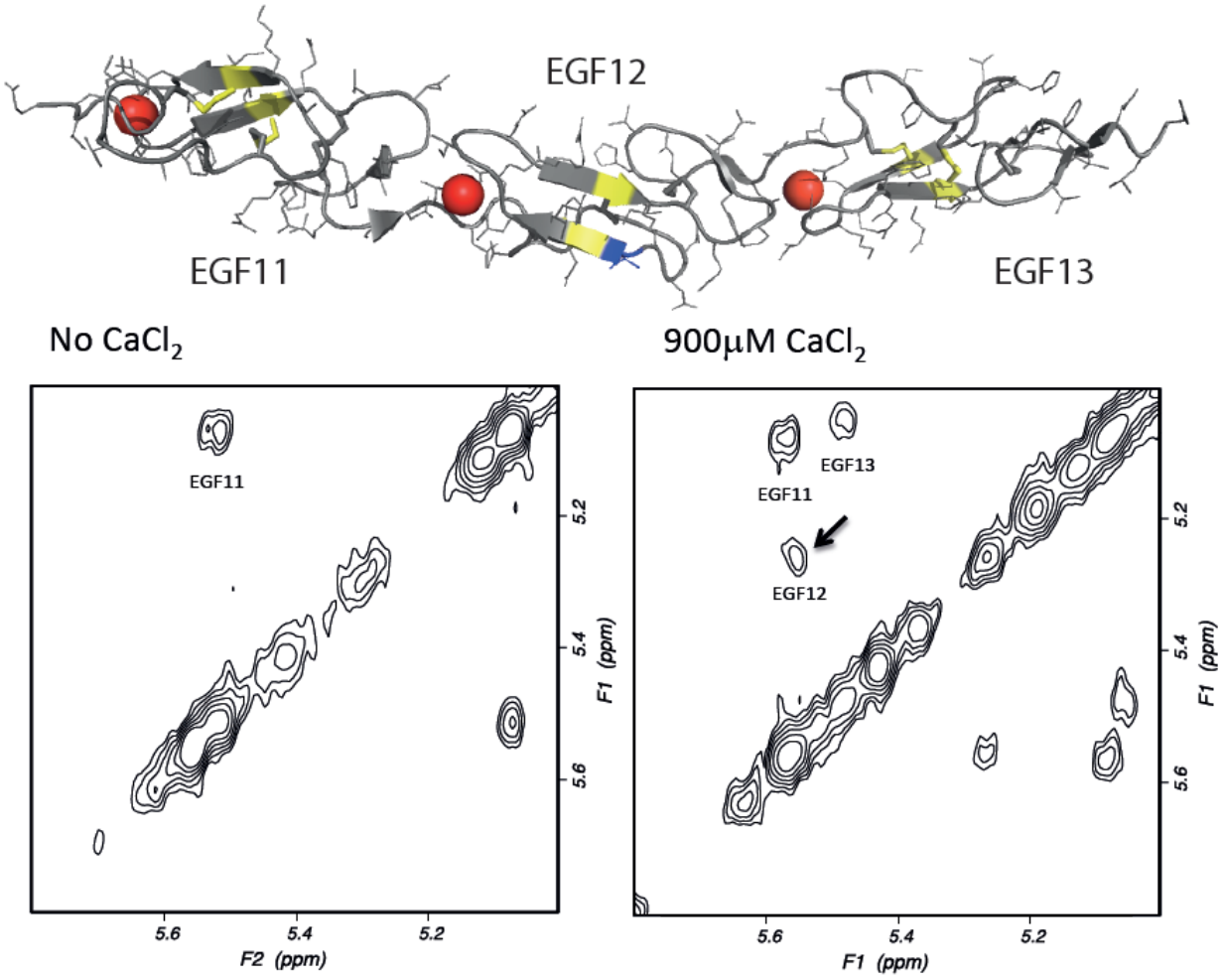

Figure S11 NMR analysis of the calcium dependence of the major β-hairpin in hN1$_{11-13}$ Antiparallel β–sheet is characterised by downfield shifted Hα resonances and by short distances between Hα protons on opposite strands. In NOE spectra, this close proximity gives rise to observable Hα-Hα NOE cross peaks; these interactions are not observed in any other type of secondary structure or in unstructured regions of proteins. In the major β-hairpin in calcium-binding EGF domains, the Hα protons of the 3rd and 4th cysteine residue are in close proximity. In the panel on the right, collected for N1$_{11-13}$ with 900µM $CaCl_2$, Hα-Hα NOEs are observed for this pair of cysteines in EGF11 (C429-C438) , EGF12 (C467-C476, arrowed) which contains the ligand-binding region, and EGF13 (C505-C514) indicating a stable antiparallel β-sheet in the presence of calcium in each of the domains. In the panel on the left, collected for N1$_{11-13}$ in the absence of calcium, an Hα-Hα NOE is only observed for EGF11. This suggests that in the absence of calcium, the β-sheet in EGF11 is stable while the β-sheet in EGF12 and EGF13 is not present. This confirms the important role that calcium plays in stabilising the major β-hairpin of EGF12 and EGF13. The unmodified structure (2VJ3.pdb) is shown highlighting the secondary structure with the calcium ions in red, T466 in blue and the cysteine residues which give rise to the Hα-Hα NOEs, in yellow.

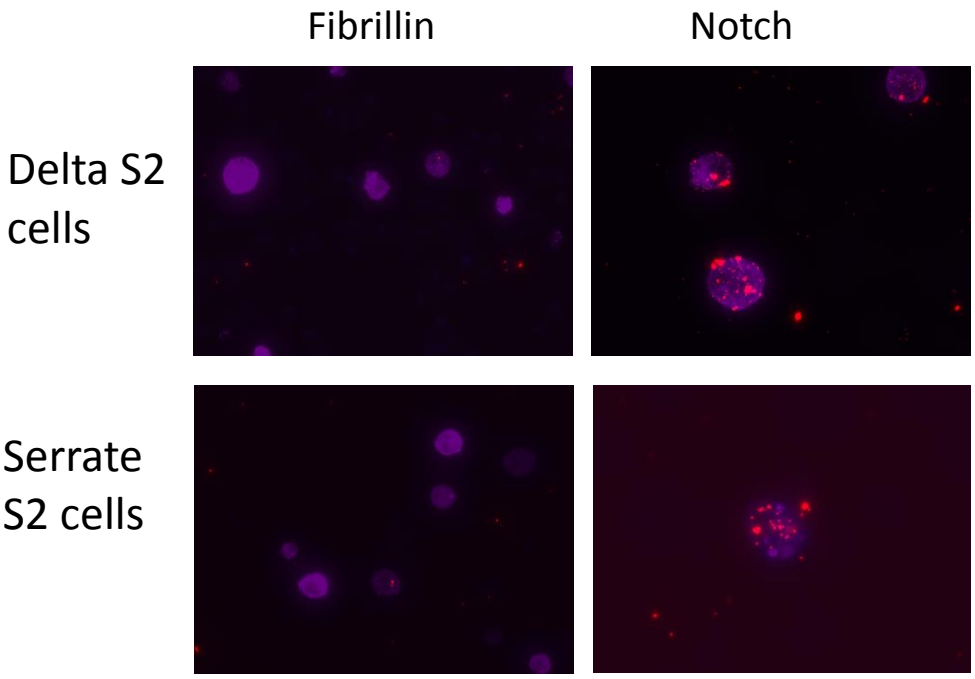

Figure S12 Immunofluorescence images of the interaction between protein-coated fluorescent beads and Notch ligand-expressing cells. *Drosophila* S2 cells expressing a C-terminal V5 tagged Delta or Serrate as previously described (Whiteman et al,. 2013 J.Biol.Chem. 288, 7305-7312) are shown interacting with biotinylated *Drosophila* Notch $_{11\text{-}13}$ coupled to Avidin Coated Fluorescent Beads (Spherotech). The samples were mounted on glass plates, fixed, permeablised, and stained with rabbit anti-V5 (Bethyl Laboratories, 1:1,000), followed by anti-rabbit Cy5 (Jackson Immunoresearch Laboratories, 1:600). Images were captured using a cooled digital camera (Hamamatsu) on a Zeiss Axiovert microscope with a Z spacing of 0.5 μm, and processed and overlaid using Openlab (Improvision). Cy5 signal was obtained at 690/50 nm (Filter Set 50), the signal of the fluorescent beads was obtained at 630/75 nm (Filter Set 45). Fluorescent beads (shown in red) coated with *Drosophila* Notch$_{11\text{-}13}$ showed binding to S2 cells expressing Delta or Serrate (both shown in purple), while beads coated with a control fibrillin-1 triple EGF domain construct did not. For clarity, unbound beads have been washed off prior to visualization.